

## Article

# An Integrating Framework for Biomass and Carbon Stock Spatialization and Dynamics Assessment Using Unmanned Aerial Vehicle LiDAR (LiDAR UAV) Data, Landsat Imagery, and Forest Survey Data in the Mediterranean Cork Oak Forest of Maamora

Sanaa Fadil <sup>1,2,\*</sup>, Imane Sebari <sup>1</sup> , Moulay Mohamed Ajerame <sup>3</sup>, Rayhana Ajeddour <sup>1</sup>, Ibtihal El Maghraoui <sup>1</sup>, Kenza Ait El kadi <sup>1</sup> , Yahya Zefri <sup>1</sup> and Mouad Jabrane <sup>1</sup>

<sup>1</sup> Cartography and Photogrammetry Department, School of Geomatics and Surveying Engineering (Hassan II Institute of Agronomy and Veterinary Medicine), Rabat 10000, Morocco; i.sebari@iav.ac.ma (I.S.); k.aitelkadi@iav.ac.ma (K.A.E.k.); m.jabrane@iav.ac.ma (M.J.)

<sup>2</sup> National Agency of Water and Forests, Rabat 10000, Morocco

<sup>3</sup> Department of Statistics and Applied Computer Science, IAV Hassan II, Rabat 10000, Morocco

\* Correspondence: s.fadil@iav.ac.ma; Tel.: +212-648770740

**Abstract:** Spatialization of biomass and carbon stocks is essential for a good understanding of the forest stand and its characteristics, especially in degraded Mediterranean cork oak forests. Furthermore, the analysis of biomass and carbon stock changes and dynamics is essential for understanding the carbon cycle, in particular carbon emissions and stocks, in order to make projections, especially in the context of climate change. In this research, we use a multidimensional framework integrating forest survey data, LiDAR UAV data, and extracted vegetation indices from Landsat imagery (NDVI, ARVI, CIG, etc.) to model and spatialize cork oak biomass and carbon stocks on a large scale. For this purpose, we explore the use of univariate and multivariate regression modeling and examine several types of regression, namely, multiple linear regression, stepwise linear regression, random forest regression, simple linear regression, logarithmic regression, and quadratic and cubic regression. The results show that for multivariate regression, stepwise regression gives good results, with  $R^2$  equal to 80% and 65% and RMSE equal to 2.59 and 1.52 Mg/ha for biomass and carbon stock, respectively. Random forest regression, chosen as the ML algorithm, gives acceptable results, explaining 80% and 60% of the variation in biomass and carbon stock, respectively, and an RMSE of 2.74 and 1.72 Mg/ha for biomass and carbon stock, respectively. For the univariate regression, the simple linear regression is chosen because it gives satisfactory results, close to those of the quadratic and cubic regressions, but with a simpler equation. The vegetation index chosen is ARVI, which shows good performance indices, close to those of the NDVI and CIG. The assessment of biomass and carbon stock changes in the study area over 35 years (1985–2020) showed a slight increase of less than 10 Mg/ha and a decrease in biomass and carbon stock over a large area.

**Keywords:** biomass; carbon stock; dynamics; modeling regression; spatialization; random forest; LiDAR UAV; Landsat images; cork oak; Maamora forest



**Citation:** Fadil, S.; Sebari, I.; Ajerame, M.M.; Ajeddour, R.; El Maghraoui, I.; Ait El kadi, K.; Zefri, Y.; Jabrane, M. An Integrating Framework for Biomass and Carbon Stock Spatialization and Dynamics Assessment Using Unmanned Aerial Vehicle LiDAR (LiDAR UAV) Data, Landsat Imagery, and Forest Survey Data in the Mediterranean Cork Oak Forest of Maamora. *Land* **2024**, *13*, 688. <https://doi.org/10.3390/land13050688>

Academic Editor: Le Yu

Received: 23 March 2024

Revised: 25 April 2024

Accepted: 2 May 2024

Published: 14 May 2024



**Copyright:** © 2024 by the authors. Licensee MDPI, Basel, Switzerland. This article is an open access article distributed under the terms and conditions of the Creative Commons Attribution (CC BY) license (<https://creativecommons.org/licenses/by/4.0/>).

## 1. Introduction

Deforestation, desertification and climate change are among the major challenges facing humanity in the 21st century. Forest ecosystems, which cover about 31% of the world's land area [1], play a crucial role in the global carbon cycle, storing 56% of the world's carbon [2] and thus helping to mitigate climate change. In fact, they contribute significantly to this process, accounting for about 80% of aboveground carbon and 40% of belowground terrestrial carbon [3]. Unfortunately, terrestrial ecosystems are vulnerable to

carbon losses due to land degradation, forest fires, storms and pest outbreaks [4]. These losses are expected to contribute to a decline in the terrestrial carbon sink [5]. In fact, about 5–10 Gt CO<sub>2</sub> per year are lost through deforestation and forest degradation [6].

Usually, biomass and carbon stock estimation is based exclusively on field surveys and allometric equations developed in the same forest. However, this approach is time consuming, laborious and cannot be applied to large areas. Remote sensing overcomes these drawbacks by being more efficient, time-saving and applicable to large areas. In fact, remote sensing with its various techniques (satellite imagery, LiDAR, UAV, SAR, aerial photography..., etc.) is widely used for biomass and carbon stock estimation and mapping all over the world [7–9]. Satellite imagery allows large scale biomass and carbon stock analysis, but does not provide sufficient information on stand structure as it does not penetrate the canopy, unlike LiDAR (Light Detection And Ranging). This technology provides high quality information on forest stands, but over a limited area [7,10–14]. It has revolutionized biomass estimation from satellites [15,16]. Large-scale LiDAR remote sensing far exceeds the ability of radar and optical sensors to estimate carbon stocks for all forest types [17]. It can be mounted on space, airborne, or ground platforms, each platform serving specific forest inventory needs. In research studies, LiDAR data are used in conjunction with satellite imagery [18], or alone on several dates, depending on their availability. Unmanned aerial vehicles (UAVs) also have the potential to increase the efficiency of forest data collection, as they have much higher spatial and temporal resolution than other remote sensing techniques [19,20], especially with a LiDAR sensor [21]. Thus, the UAV/satellite combination quickly proved its worth by providing solutions to various scientific questions [20]. Different UAV/satellite synergies have been categorized (data comparison, multiscale elucidation, model calibration and data fusion). The approach of combining multi-sensor sources is more efficient if the uncertainties arising from the data combination are controlled [20,22].

Forest degradation is a broad term that can be divided into several definitions depending on the aspect it affects (biodiversity conservation, carbon sequestration, timber production, soil conservation, cultural values or recreation) [23]. In this study, we examine carbon stock degradation, which is defined by the Intergovernmental Panel on Climate Change as a long-term direct loss (lasting X years or more) of at least Y% of forest carbon stocks due to human activities over a time period T that does not qualify as deforestation or an activity under Article 3.4 of the Kyoto Protocol [23]. The causes of this reduction can be natural (stand ageing, forest fires, parasitic infestations, etc.) or anthropogenic (population growth, illegal logging, overgrazing, pollarding and delimiting, acorn collection, etc.).

To assess this aspect of degradation, we examine biomass and carbon stocks. Biomass is dynamic and therefore needs to be continuously monitored to provide information on the carbon cycle of the forest ecosystem (sources and sinks) [15,16,24,25]. Regular estimation and monitoring of biomass and carbon stocks (aboveground, belowground and total) over space and time are essential to understand their development and changes. In fact, a good understanding of biomass and carbon stock changes can improve forest management decisions, especially in degraded areas [26]. Furthermore, different remote sensing techniques are used to study biomass and carbon stock dynamics: Change detection approaches can use bi-temporal imagery or temporal trajectory analysis. Multi-temporal Landsat TM and machine learning algorithms are used in [27] to study aboveground forest carbon stock according to the land cover change, between 1990 and 2010. Another approach is used to map biomass changes between 1998 and 2018 in the mangrove forest in the coastal area of Thai Binh, using regression models between field values of AGB and some spectral indices (NDVI, SAVI, GNDVI) [28]. Landsat images (MSS (multispectral scanner), ETM+ (thematic mapper), and OLI (operational land imager)) are used to classify the study area into different ecosystem units for the years 1975, 2000, and 2020, then to investigate the ecosystem service values (ESVs) and analyze the dynamic pattern of carbon sequestration using the InVEST model [29]. A dataset consisting of Landsat TM5, ETM+ multispectral imagery, HJ-1 multispectral imagery, and China Environmental Disaster

Reduction Satellite (HJ-1) multispectral images are used in Zoigê alpine grassland to assess the carbon stocks, for three periods from 2000 to 2020, using the InVEST model [30]. Aerial photography is also used to assess biomass and carbon stock dynamics. Based on multi-temporal photogrammetric measurements, dendrometric parameters, in particular crown height and diameter, are estimated and integrated into corresponding allometric equations to estimate the biomass value [31]. Another approach based on a regression between parameters from the canopy height model (CHM) derived from aerial photographs and the AGB from field measurements to estimate biomass [32] is tested in a seasonal tropical forest. Synthetic Aperture Radar (SAR) or Interferometric Synthetic Aperture Radar (InSAR), has a high sensitivity to the forest vertical structure, and thus it is widely used in the estimation and dynamic monitoring of canopy heights [33]. Indeed, changes in biomass and carbon stocks can be recovered directly from height changes. In this study [24], SAR data ALOS PALSAR (Advanced Land Observing Satellite's Phased Array-type L-band Synthetic Aperture Radar), and ALOS-2 PALSAR-2 polarizations and Sentinel-1(C-band) data, are used to build AGB models for 2007, 2009 and 2016, and then validated by field data combined with LiDAR data. A change analysis is performed, comparing the three biomass maps. In order to overcome the weaknesses of SAR technology, some researchers have used interferometric SAR (InSAR), which can provide 3D data [34]. LiDAR data are also used in biomass and carbon stock dynamics studies. Indeed, multi-temporal airborne LiDAR data are used for the estimation of AGB changes [10], in comparing direct and indirect methods. Other studies used multi-temporal airborne LiDAR to estimate AGB changes in Panama [35], and in Borneo [36]. Multitemporal airborne LiDAR (ALS) data combined with field inventory, are used to estimate carbon stock change between 2002 and 2012 at the Landscape forest, Scotland, United Kingdom [37]. A combination of satellite imagery and LiDAR data are exploited to estimate carbon stock changes in Auckland, New Zealand [38]. In this research, plot-level AGC stocks were linked with vegetation spectral/structural features derived from Landsat images and LiDAR data. Another study exploited a method based on the combination of annual Landsat image time series and high-density airborne LiDAR data to characterize carbon stock variability [39]. RapidEye imageries, Chronological LANDSAT imageries, and LiDAR data are used for the classification of types of tree species and estimation of carbon stock changes [40].

Recently, Machine learning regression has become extremely important in biomass and carbon stock estimation and has proved its efficiency in modeling trees and soil carbon stock and its spatialization [41,42]. These techniques can be used to assess and analyze the contribution of various factors (Climatic, Edaphic, Topographical. . . , etc) acting in a complex manner and consequently, evaluating complex nonlinear relationships between satellite sensor reflectance and ecosystem [41,43]. We distinguish several ML algorithms such as support vector machine (SVM), k-nearest neighbors (KNN), and Random Forest (RF). For biomass modeling and prediction, Random Forest regression has been tested widely these recent years in different ecological conditions. Effectively, it was superior to the traditional regression model in AGB modeling in the grassland of Xilin Gol League [44], it is used to construct the estimation model of grassland AGB in eastern Inner Mongolia based on field data, MODIS (MOD13Q1) data and environmental data (climate and topography) [45] and is used to predict forest volume and biomass in two regional study areas (Spain and Norway) based on remotely sensed auxiliary data obtained from multiple sensors. Random forest regression is also used to assess aboveground forest biomass (AGB) changes in a Mediterranean forest context, using ALOS-PALSAR, Sentinel 1, and Landsat 8 data [46].

As mentioned above, several research methodologies have been developed to assess temporal changes in the biomass and carbon stock of a forest stand. Furthermore, the choice of the appropriate methodology depends on the availability of LiDAR data, old satellite images and the specific characteristics of the forest stand under study. In this research, the species studied is cork oak. *Quercus* species have a very wide distribution, from Mediterranean semi-desert woodlands to subtropical rainforests in Europe, North America and Southeast Asia [47] and cork oak (*Quercus suber*) is endemic to the Mediterranean

basin [48]. Few studies have focused on the biomass and carbon stock of this species, despite its major contribution to carbon sequestration, through all the components of the tree but also through the cork that is specific to it [48]. Therefore, the study of biomass and carbon stocks of Mediterranean cork oak in a degraded Mediterranean forest using traditional methods is not feasible. For these reasons, in this research work, we explored an integrated approach using LiDAR-UAV data, extracted vegetation indices Landsat imagery and field survey data to spatialize and map biomass and carbon stock at the landscape scale and then assess their dynamics over 35 years.

The general objective is to spatialize biomass and carbon stocks on a large scale and to analyze their dynamics using an innovative methodological approach, and the specific objectives are: (i) to explore the potential of vegetation indices from Landsat imagery in biomass and carbon stock modelling, (ii) to analyze and compare different regression types including ML techniques (Random Forest Regression), (iii) to assess biomass and carbon stock changes in Mediterranean cork oak forest stands.

## 2. Materials and Methods

The methodology of this research work is organized in three phases: in the first phase, using forest survey and extracted LiDAR UAV metrics, a LiDAR UAV-based biomass and carbon stock model is developed (Model 1), the details of which are presented in the paper “Modeling and spatialization of biomass and carbon stock using unmanned aerial vehicle LiDAR (LiDAR UAV) metrics in cork oak forest of Maamora.” In the second phase, another model (Model 2) is developed using biomass and carbon stock maps of LiDAR UAV surveys and vegetation indices of Landsat 8 images. In the third phase, a biomass and carbon stock distribution mapping of 1985 and 2020 will be carried out, then the changes between these two years assessed (Figure 1).

### 2.1. Study Area

The Maamora forest is a Moroccan cork oak forest of approximately 134,000 ha [49], with cork oak as the main species, covering 60,000 ha. This area is characterized by a subhumid bioclimate in its western part and semiarid one in its central and eastern parts. It plays many environmental, social, and economic roles, including carbon sequestration through its biomass. Our study was carried out in central canton C, group III, parcels 10 and 6, inside a pure adult cork oak stand (Figure 2).

### 2.2. LiDAR UAV-Based Biomass and Carbon Stock Models (Model 1)

In this section, a model (Model 1) is developed to spatialize biomass and carbon stock in the LiDAR UAV surveys. LiDAR UAV data are collected using unmanned aerial vehicle DJI Matrice 600 pro equipped with Velodyne VLP-16 LiDAR sensor in three survey areas (ALS1, 2, and 3), covering approximately 30 ha at different locations in Canton C. The LiDAR UAV point cloud data were collected at a range accuracy of 3 cm, and a data rate of 300,000 points per second. Field survey data (circumference 1.3 m, tree height, and plot center coordinates) are also collected in 31 plots randomly distributed across the three LiDAR UAV surveys. Then, the total tree biomass and carbon stock are estimated using allometric equations described in [7,48] and LiDAR UAV data are preprocessed and processed to obtain metrics. Finally, modeling biomass and carbon stock using LiDAR UAV data is performed using different regression types. The best model is selected and applied to spatialize biomass and carbon stock in the three LiDAR UAV surveys. Using the biomass and carbon stock maps resulting from this stage, we can conclude the biomass and carbon stock of each pixel on the three ALS UAV surveys (Bpixel and Cpixel). The detailed methodology of this part is presented in the article “Modeling and spatialization of biomass and carbon stock using unmanned aerial vehicle LiDAR (LiDAR UAV) metrics in cork oak forest of Maamora” and in Figure 1, Phase 1.

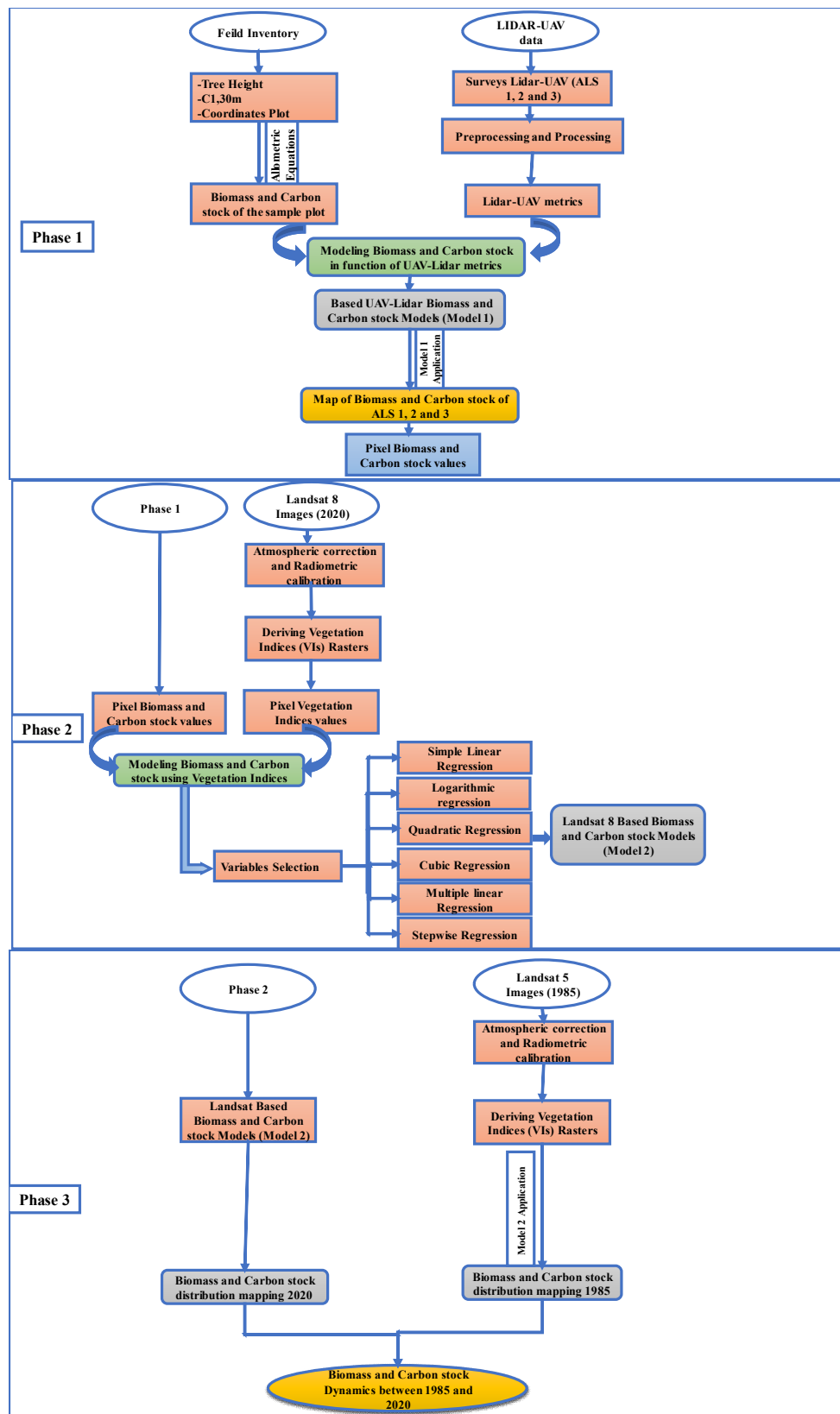
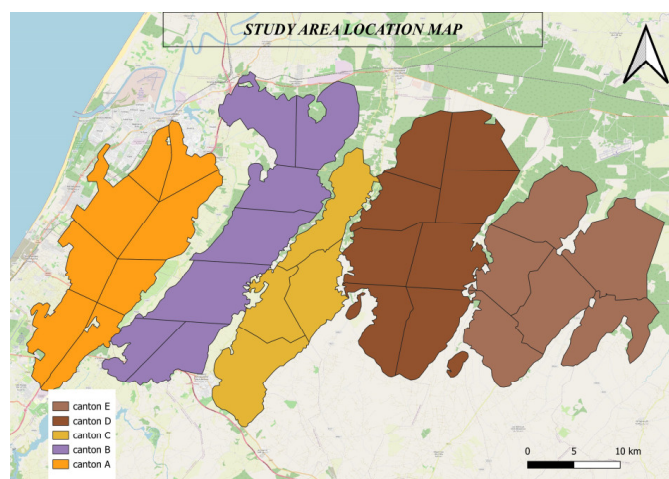


Figure 1. Flowchart of the research method.



(a)



(b)

**Figure 2.** (a) Study area location map; (b) Maamora cork oak stand.

### 2.3. Landsat Image Acquisition and Preprocessing

To study biomass and carbon stock changes in the long term, we chose the years 1985 and 2020. Landsat 4 and 8 images with a high spatial resolution of 30 m are used for 1985 and 2020, respectively, for the same time of the year (October). This month is chosen to avoid the effect of abundant herbaceous vegetation. The chosen cloud cover is minimal to nonexistent. The choice of Landsat sensor is related to the availability of older images needed for our study. Landsat 4 and 8 data were retrieved from the United States Geological Survey (USGS) Earth Explorer website (<https://earthexplorer.usgs.gov/>), accessed 29 January 2024, from Landsat 4-5 Thematic Mapper Collection 2 Level-1 data and Landsat 8-9 Operational Land Imager (OLI) and Thermal Infrared Sensor (TIRS) Collection 2 Level-1. The Landsat image is pre-processed with atmospheric correction and radiometric calibration.

### 2.4. Multidimensional Image Composite of Biomass and Carbon Stocks

Different vegetation indices exist in the literature (about 150) [41]. In this study, we selected nine (Table 1), due to their performance in estimating biomass and carbon stock in previous studies. A composite image is produced by superimposing the images corresponding to the selected vegetation indices and the LiDAR UAV-based biomass and carbon stock maps. A pixel sample is selected in the image dataset by removing all outlier values.

**Table 1.** List of vegetation indices derived from Landsat 8 image and their formulae.

Vegetation Index	Description	Formula	Reference
ARVI	Atmospheric Resistant Vegetation Index	$RNIR - (2 RRed - RBlue)/RNIR + (2 RRed - RBlue)$	[50]
TVI	Triangular Vegetation Index	$0.5 \times [120 \times (RNIR - RGreen) - 200 \times (RRed - RGreen)]$	[51]
CIG	Chlorophyll Index Green	$(RNIR/RRed) - 1$	[52]
DVI	Difference Vegetation Index	$RNIR/RRed$	[53]
EVI	Enhanced Vegetation Index	$(2.5 \times (RNIR - R))/(RNIR + 6 \times RRed - 7.5 \times RBlue + 1)$	[54]
NDVI	Normalized Difference Vegetation Index	$(RNIR - RRed)/(RNIR + RRed)$	[55]
GNDVI	Green Normalized Difference Vegetation Index	$(RNIR - RGreen)/(RNIR + RGreen)$	[56]
OSAVI	Optimized Soil Adjusted Vegetation Index	$(RNIR - RRed)/(RNIR + RRed + 0.16)$	[57]
SAVI	Soil Adjusted Vegetation Index	$1.5 (RNIR - RRed)/(RNIR + RRed + 0.5)$	[58]

### 2.5. Spatial Modeling of Cork Oak Biomass and Carbon Stock

Before performing modeling regression, it is interesting to study the correlation between the biomass and carbon stock and the vegetation indices to examine the relationship between them and to select the most correlated. In this study, the Pearson correlation coefficient is used. Many researchers have studied the correlation between vegetation indices and biomass and carbon stock [8,12,14]. Regression analysis assessed the relationship between biomass and carbon stock and vegetation indices (VIs). Based on the correlation result, a multivariate regression is first performed between the Bpixel and Cpixel and the nine vegetation indices using multiple and stepwise linear regression and random forest, which is a machine learning regression, then a univariate regression is performed with a single vegetation index (the most correlated) through different functions: linear, logarithmic, quadratic, and cubic regression.

In the above analysis, the Bpixels and Cpixels are the dependent variables and the VIs are the independent or explanatory variables. To assess the accuracy of the models, we calculated three commonly used indicators [41]: coefficient of determination ( $R^2$ ), root mean square error (RMSE) and mean square error (MSE). The best-fitting model has the highest  $R^2$  and the lowest RMSE and MSE. These indicators are as follows:

$$r = \sqrt{R^2} = \sqrt{1 - \frac{\sum_{i=1}^n (y - \bar{y})^2}{\sum_{i=1}^n (\hat{y} - \bar{y})^2}} \quad (1)$$

$$RMSE = \sqrt{\frac{\sum_{i=1}^n (\hat{y} - y)^2}{n}} \quad (2)$$

$$rRMSE = \frac{RMSE}{\bar{y}} \quad (3)$$

$$MAE = \frac{1}{n} \sum_{i=1}^n |\hat{y} - y| \quad (4)$$

where  $y$  is the field-based biomass and carbon stock estimates (observed),  $\bar{y}$  is the mean of  $y$ ,  $\hat{y}$  is the estimated biomass and carbon stock, and the number of testing datasets utilized for the evaluation is denoted by  $n$ .

Multicollinearity between independent variables presents an issue in model development [41]. The variance inflation factor (VIF), is then used to evaluate multicollinearities, which quantifies the degree and correlation between explanatory variables.

The ML regression method used in this study is random forest regression. For this analysis, data are divided into training data (70%) and testing data (30%), with a default number of trees equal to 500 ( $n_{tree} = 500$ ), and we will also check if this default number was sufficient, visualizing the error rates or MSE of a random forest object [59]. In order to understand the contribution of the different vegetation indices in the random forest model

for biomass and carbon stock, we then present their importance graphically. Two measures of variable importance are reported. The first is based on the average decrease in prediction accuracy on the out-of-bag samples when a given variable is excluded from the model (% IncMSE). The second is a measure of the total decrease in node impurity resulting from splitting over that variable, averaged over all trees (IncNodePurity) [60].

2.6. Spatialization of Cork Oak Biomass and Carbon Stock

Before applying the model, we restricted the map space using a vegetation mask [25]. Two classes are identified in the study area—ground and vegetation (cork oak stand). The selected regression model based on R<sup>2</sup>, RMSE, and MSE is used to make predictions for all cork oak 30 m pixels across the study area.

3. Results

3.1. Correlation between Biomass/Carbon Stock and VIs

The Pearson correlation coefficient of all vegetation indices (VIs) examined in this study is almost equal. All vegetation indices (VIs) showed a strong correlation with biomass and carbon stock at pixel level (Table 2). In fact, the most highly correlated VI is ARVI, followed by NDVI, DVI and CIG, then OSAVI, EVI and finally SAVI, TVI and GNDVI. Several studies have shown a strong correlation between vegetation indices and biomass/carbon stocks, whether extracted from Sentinel imagery [61], Landsat, or other sources.

Table 2. Coefficient correlation between biomass/carbon stock and vegetation indices.

Dependent Variables	Vegetation Indices									
	ARVI	TVI	CIG	DVI	EVI	GNDVI	NDVI	OSAVI	SAVI	
Btree–Total	0.897	0.813	0.894	0.894	0.853	0.812	0.894	0.873	0.812	
Cst–total	0.808	0.672	0.799	0.799	0.722	0.677	0.791	0.749	0.670	

3.2. Biomass and Carbon Stock Model Development

Biomass and carbon stock modeling was carried out using multivariate and univariate regression.

3.2.1. Biomass and Carbon Stock Multivariate Regression Modeling

The multivariate regression of biomass and carbon stock is investigated using three types of regression: multiple linear regression, stepwise linear regression, and machine learning random forest regression.

The results of the biomass and carbon stock regressions show that R<sup>2</sup> is almost the same for the three regression types. For biomass, the values are 0.81 for multiple linear regression and 0.80 for stepwise linear and random forest regression, which means that multiple linear, stepwise linear and random forest regression explain 80% to 81% of the variation in biomass in the study area (Tables 3 and 4). For carbon stock, the values are 0.69, 0.65 and 0.60 for multiple linear regression, stepwise linear regression and random forest regression respectively, which means that multiple linear regression, stepwise linear regression and random forest regression explain 60% to 69% of the variation in carbon stock in the study area.

Table 3. Model development table with performance indices.

	Model Regression	Model Equation	R <sup>2</sup>	Adjusted R <sup>2</sup>	RMSE (Mg/ha)	MSE (Mg/ha)	
B <sub>tree–Total</sub>	Multiple linear regression	B <sub>tree–Total</sub> = 28.338 + 228.21ARVI – 4384CIG – 662.785EVI – 59.463GNDVI – 600.377OSAVI + 1210.754SAVI (5)	0.81 *	0.79	2.55	6.50	
	Stepwise regression	B <sub>tree–Total</sub> = –0.274 + 66.411 × ARVI (6)	0.80 *	0.80	2.59	6.70	
	Simple linear regression	B <sub>tree–Total</sub> = –0.274 + 66.411 × ARVI (7)	0.80 *	0.80	2.59	6.70	
		B <sub>tree–Total</sub> = 2.051 + 5.723 × NDVI (8)	0.80 *	0.79	2.63	6.90	
		B <sub>tree–Total</sub> = –9.716 + 20.615 × CIG (9)	0.80 *	0.79	2.62	6.91	
	Logarithmic	B <sub>tree–Total</sub> = 32.532 + 11.448 ln (ARVI) (10)	0.78 *	0.77	2.77	7.69	
		B <sub>tree–Total</sub> = 48.873 + 33.867 ln (NDVI) (11)	0.79 *	0.78	2.68	7.18	
		B <sub>tree–Total</sub> = 11.456 + 22.219 ln (CIG) (12)	0.79 *	0.79	2.65	7.00	
	Quadratic	B <sub>tree–Total</sub> = 0.582 + 56.154 ARVI + 25.787ARVI <sup>2</sup> (13)	0.80 *	0.80	2.58	6.68	
		B <sub>tree–Total</sub> = –12.075 + 42.403 NDVI + 80.949NDVI <sup>2</sup> (14)	0.80 *	0.79	2.62	6.86	
		B <sub>tree–Total</sub> = –13.848 + 28.365 CIG – 3.448CIG <sup>2</sup> (15)	0.80 *	0.79	2.62	6.86	
	Cubic	B <sub>tree–Total</sub> = –2664 + 114.779ARVI – 281.301ARVI <sup>2</sup> + 488.904 ARVI <sup>3</sup> (16)	0.80 *	0.79	2.59	6.65	
		B <sub>tree–Total</sub> = –7.256 + 203.413NDVI <sup>2</sup> – 116.219NDVI <sup>3</sup> (17)	0.80 *	0.79	2.62	6.86	
		B <sub>tree–Total</sub> = –12.59 + 24.687CIG – 1.039CIG <sup>3</sup> (18)	0.80 *	0.79	2.62	6.86	
	C <sub>st–total</sub>	Multiple linear regression	C <sub>st–total</sub> = 26.298 + 102.979ARVI + 11.546CIG – 342.602EVI1 – 37.787GNDVI1 – 408.949OSAVI + 634.477SAVI1 (19)	0.69 *	0.66	1.43	2.05
		Stepwise regression	C <sub>st–total</sub> = –0.378 + 26.232 ARVI (20)	0.65 *	0.65	1.52	2.30
Simple linear regression		C <sub>st–total</sub> = –0.378 + 26.232 ARVI (21)	0.65 *	0.64	1.52	2.30	
		C <sub>st–total</sub> = –8.605 + 38.395 NDVI (22)	0.62 *	0.62	1.58	2.49	
		C <sub>st–total</sub> = –4.035 + 8.078 CIG (23)	0.63 *	0.63	1.55	2.40	
Logarithmic		C <sub>st–total</sub> = 12.400 + 4415 ln(ARVI) (24)	0.60 *	0.59	1.63	2.65	
		C <sub>st–total</sub> = 18.672 + 13.031 ln(NDVI) (25)	0.60 *	0.60	1.61	2.59	
		C <sub>st–total</sub> = 4.271 + 8.588 ln(CIG) (26)	0.61 *	0.61	1.59	2.53	
Quadratic		C <sub>st–total</sub> = 1800 + 0.152 ARVI + 65.570 ARVI <sup>2</sup> (27)	0.67 *	0.66	1.47	2.17	
		C <sub>st–total</sub> = 7.06 – 53.356NDVI + 131.227NDVI <sup>2</sup> (28)	0.64 *	0.63	1.54	2.37	
		C <sub>st–total</sub> = –0.325 + 1.119CIG + 3.096CIG <sup>2</sup> (29)	0.64 *	0.63	1.54	2.36	
Cubic		C <sub>st–total</sub> = –1018 + 51.048ARVI – 201.032ARVI <sup>2</sup> + 424.447ARVI <sup>3</sup> (30)	0.67 *	0.66	1.46	2.14	
		C <sub>st–total</sub> = 1.140 – 26.506 NDVI <sup>2</sup> + 153.042 NDVI <sup>3</sup> (31)	0.64 *	0.63	1.54	2.36	
		C <sub>st–total</sub> = –0.325 + 1.119CIG + 3.096CIG <sup>2</sup> (32)	0.64 *	0.63	1.54	2.36	

\* *p*-values are less than 0.001.

**Table 4.** Random forest regression with performance indices.

	Model Regression	Number of Variables Tried at Each Split (mtry)	ntree	R <sup>2</sup>	RMSE (Mg/ha)	MSE (Mg/ha)
<b>Btree—Total</b>	Random Forest	2	500	80.35	2.74	7.53
<b>Cst—total</b>	Random Forest	2	500	60.04	1.72	2.97

In addition, to better analyze the results, the RMSE and MSE are used, which provide information on the error between the values predicted by the model and the real values. For the biomass regression, the RMSE values indicate that the multiple linear regression is the best option, followed by the stepwise linear regression and then the random forest regression with 2.55, 2.59, and 2.74 Mg/ha respectively (Tables 3 and 4). Furthermore, for carbon stock regression, the RMSE values indicate that multiple linear regression is the best option, followed by stepwise linear regression and then random forest regression with 1.43, 1.52, and 1.72 Mg/ha respectively. However, the study of multicollinearity between the independent variables (VIs) using the variance inflation factor (VIF) shows that there is high multicollinearity, and consequently the multiple linear regression model is rejected. The details of the VIF results are presented in Tables 5 and 6. Consequently, the stepwise regression model of biomass and carbon stock presents interesting results, and we selected a vegetation index: the atmosphere resistant vegetation index (ARVI).

**Table 5.** Stepwise linear regression variance inflation factor.

		Coefficients										
Model		Non-Standardized Coefficients		Standardized Coefficients	t	Sig.	Correlations			Collinearity Statistics		
		B	Standard Error	Beta			Simple Correlation	Partial	Partial	Tolerance	VIF	
C <sub>st</sub> —total	(Constant)	−0.378	0.485		−0.779	0.438						
	ARVI	26.232	2.207	0.808	11.884	0.000	0.808	0.808	0.808	1	1	
B <sub>tree</sub> —total	(Constant)	−0.274	0.829		−0.331	0.742						
	ARVI	66.411	3.768	0.897	17.624	0.000	0.897	0.897	0.897	1	1	

**Table 6.** Multiple linear regression variance inflation factor.

		Coefficients										
VIs		Non-Standardized Coefficients		Standardized Coefficients	t	Sig.	Correlations			Collinearity Statistics		
		B	Standard Error	Beta			Simple Correlation	Partial	Partial	Tolerance	VIF	
B <sub>tree</sub> —Total												
	(Constant)	28.338	27.093		1.046	0.299						
	ARVI	228.210	185.184	3.084	1.232	0.222	0.897	0.146	0.064	0.000	2324.498	
	CIG	−4.384	18.959	−0.190	−0.231	0.818	0.894	−0.028	−0.012	0.004	250.990	
	EVI	−662.785	652.588	−2.693	−1.016	0.313	0.853	−0.121	−0.053	0.000	2608.499	
	GNDVI	−59.463	71.023	−0.324	−0.837	0.405	0.812	−0.100	−0.043	0.018	55.603	
	OSAVI	−600.377	743.128	−2.830	−0.808	0.422	0.873	−0.096	−0.042	0.000	4552.620	
	SAVI	1210.754	1135.977	3.994	1.066	0.290	0.812	0.126	0.055	0.000	5212.643	

Table 6. Cont.

VIs	Coefficients									
	Non-Standardized Coefficients		Standardized Coefficients	t	Sig.	Correlations			Collinearity Statistics	
	B	Standard Error	Beta			Simple Correlation	Partial	Partial	Tolerance	VIF
	$C_{st-total}$									
(Constant)	26,298	15,216		1728	0.088					
ARVI	102,979	104,003	3173	0.990	0.326	0.808	0.118	0.066	0.000	2324.498
CIG	10,546	10,648	1043	0.990	0.325	0.799	0.118	0.066	0.004	250.990
EVI	-342,602	366,507	-3173	-0.935	0.353	0.722	-0.111	-0.062	0.000	2608.499
GNDVI	-37,787	39,888	-0.469	-0.947	0.347	0.677	-0.113	-0.063	0.018	55.603
OSAVI	-408,949	417,356	-4394	-0.980	0.331	0.749	-0.116	-0.065	0.000	4552.620
SAVI	634,477	637,988	4772	0.994	0.323	0.670	0.118	0.066	0.000	5212.643

We can conclude that the random forest regression, chosen as the ML technique, also presents good results, explaining 80% and 60% of the variation of biomass and carbon stock, respectively, and the lowest RMSE of 2.74 and 1.72 Mg/ha for biomass and carbon stock, respectively. The importance of the contribution of vegetation indices in random forest models is presented in Figure 3. This visualization shows that VIs contributes differently in these models. In the biomass model, the most influential variables are ARVI, DVI, NDVI and OSAVI. The vegetation indices CIG, EVI and SAVI contribute moderately, and the other variables (TVI and GNDVI) show low significance.

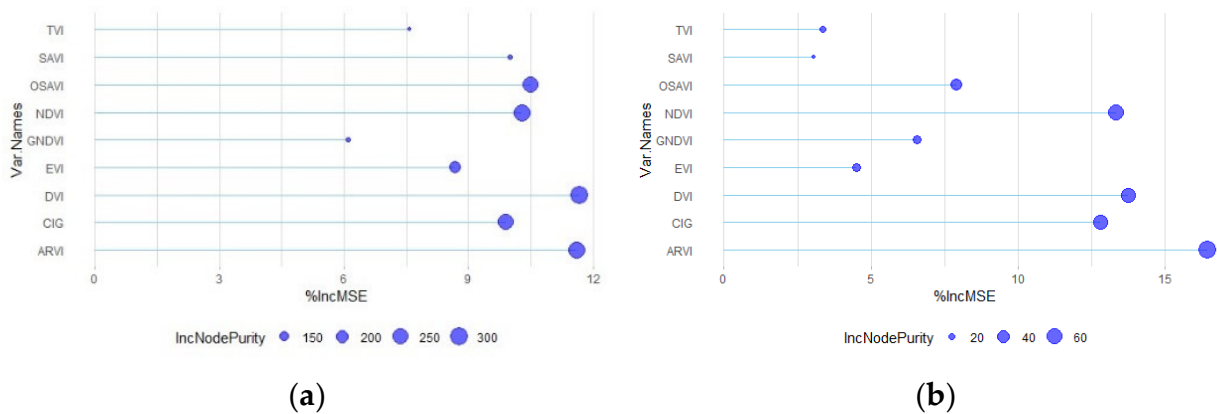
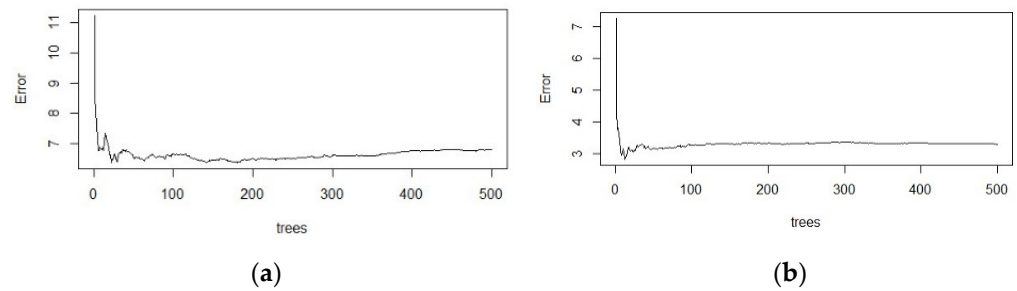


Figure 3. Model predicted variable importance: (a) biomass random forest model (b) carbon stock random forest model.

In the carbon stock model, the most influential variables are ARVI, DVI, NDVI, and CIG. The vegetation indices OSAVI and GNDVI contribute moderately, and the other variables (EVI, TVI, and SAVI) show low significance. The visualization of the error rates or MSE (Figure 4) shows that the number of trees used in this study is sufficient.



**Figure 4.** Plot of the error rates or MSE: (a) biomass random forest model (b) carbon stock random forest model.

### 3.2.2. Biomass and Carbon Stock Univariate Regression Modeling

Modeling regression between biomass/carbon stock and a single vegetation index (the most correlated: ARVI, NDVI, or CIG) is conducted using different functions: simple linear regression, logarithmic regression, quadratic and cubic regression (Figures 5 and 6).

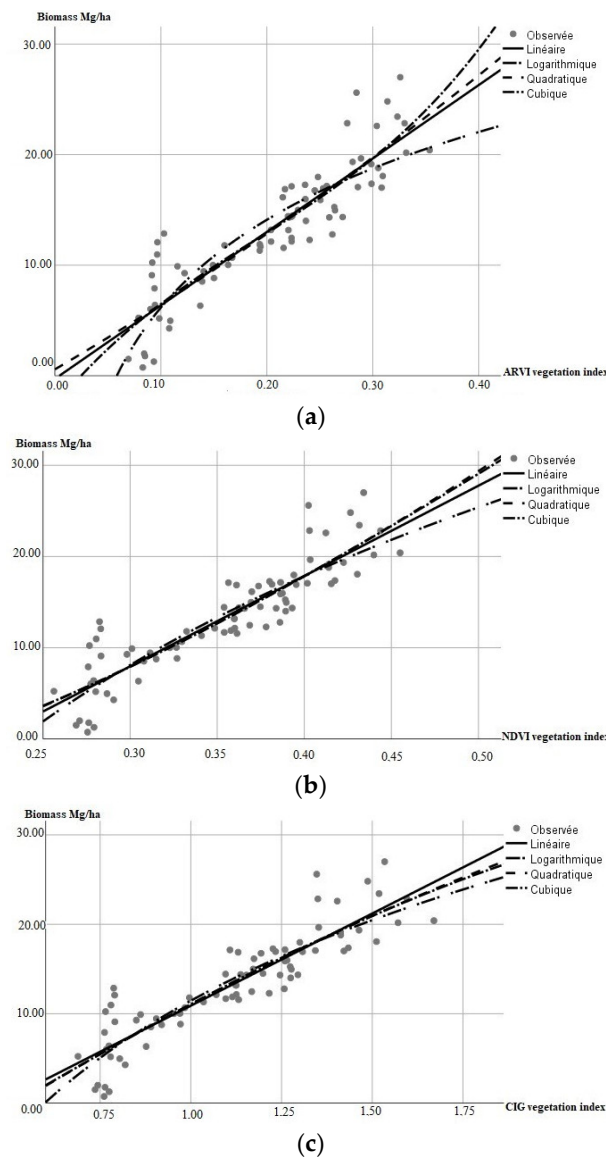


**Figure 5.** Biomass models fits of different vegetation indices with univariate regression types: (a) ARVI, (b) NDVI, (c) CIG.

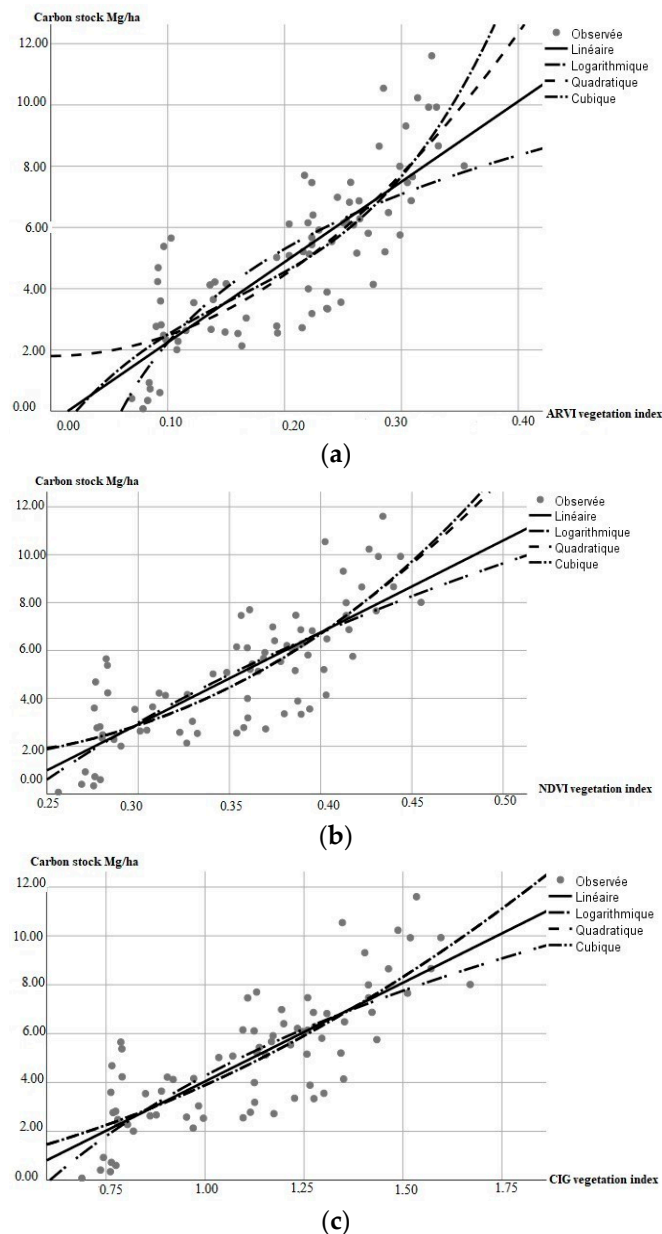


**Figure 6.** Carbon stock models fits of different vegetation indices with various regression types: (a) ARVI, (b) NDVI, CIG (c).

First, we compare these regression types for biomass and carbon stock, and then we compare the tree vegetation indices studied for the chosen regression type. For the same vegetation index, the results show that model performance indices ( $R^2$ , RMSE, and MSE) are close to each other for the four regression types (Figures 5 and 6). For the biomass model,  $R^2$  for the four regression types presents high values of between 0.78 and 0.80. In addition, comparing the other indices' performance (RMSE and MSE), the simple linear regression and cubic and quadratic regression present the lowest values, followed by logarithmic regression. This indicates that the simple linear model of ARVI, NDVI, and CIG can explain approximately 80% of the variation in biomass, while the remaining 20% was explained by other variables that were not included in the model. Details are presented in Table 3.

Regarding the carbon stock model,  $R^2$  is slightly higher for cubic and quadratic regression, with  $R^2$  between 0.64 and 0.67, followed by simple linear regression, with  $R^2$  between 0.62 and 0.65 and logarithmic regression, with  $R^2$  between 0.60 and 0.61. The other performance indices (RMSE and MSE) are relatively low for cubic and quadratic regression,

with RMSE between 1.46 and 1.54 Mg/ha, MSE between 2.14 and 2.37 Mg/ha, higher for simple linear regression with RMSE between 1.52 and 1.58 Mg/ha, MSE between 2.30 and 2.49 Mg/ha, logarithmic regression with RMSE between 1.61 and 1.63 Mg/ha and MSE between 2.53 and 2.65 Mg/ha (Table 3). The results indicate that cubic regression, quadratic and simple linear regression models of ARVI, NDVI and CIG can explain approximately between 60% and 67% of the variation in carbon stock in the study area. The model chosen in this section is the simple linear regression model because its performance indices are better than logarithmic regression and close to those of cubic and quadratic regression, except that it is simpler. This result is similar to that obtained in Section 3.2.1, where stepwise regression was chosen.

### 3.3. Biomass and Carbon Stock Spatialization

The spatialization of biomass model was carried out using Equation (6) (Table 3) in the cork oak stand of C canton, group III. Figure 7 illustrates the biomass cork oak distribution in the study area in 2020 and 1985, respectively.

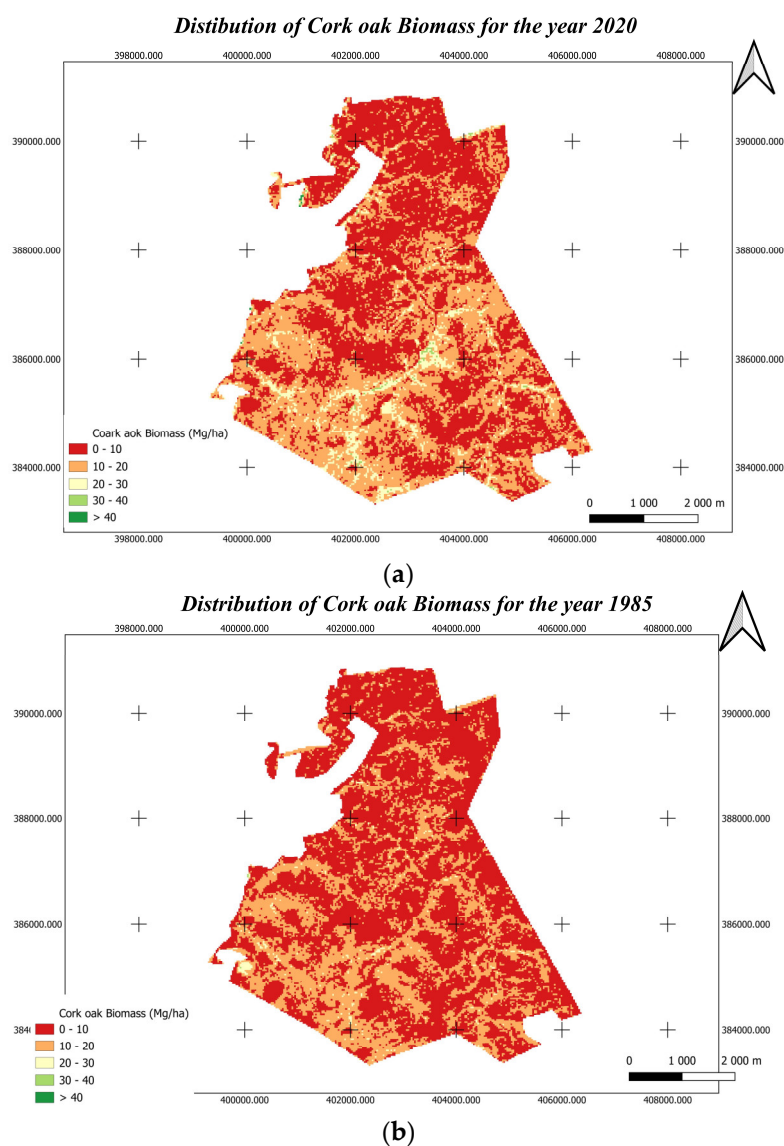
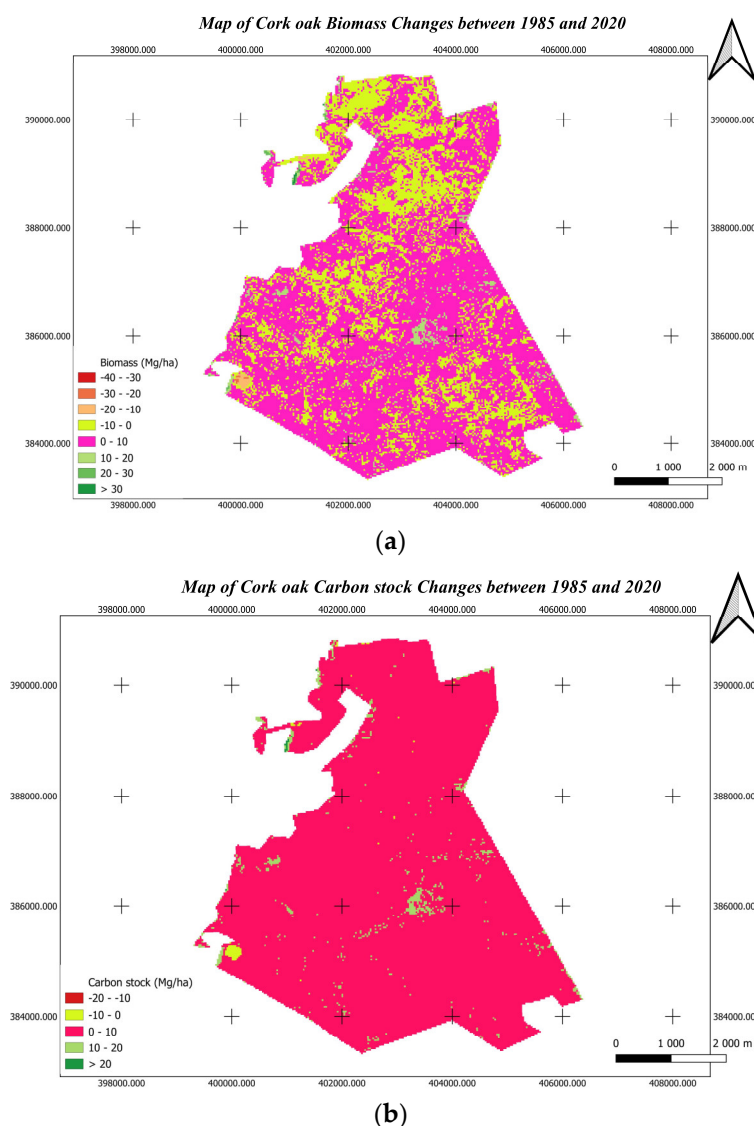


Figure 7. Distribution of cork oak biomass for 2020 (a) and 1985 (b).

In 2020, cork oak biomass ranged between 0–10 Mg/ha and 30–40 Mg/ha. The study area was dominated by very low biomass (0–10 Mg/ha), followed by an equally large area

of low biomass (10–20 Mg/ha). Moreover, the area with medium biomass (20–40 Mg/ha) was very small. In 1985, a very low biomass (0–10 Mg/ha) covered most of the surface area, followed by a low biomass (10–20 Mg/ha) and a medium biomass (20–30 Mg/ha) covering only 1% of the surface area. Biomass changes in the study area between 1985 and 2020 are illustrated in Figure 8. This figure shows that biomass has declined with (−10 to 0 Mg/ha) in approximately half the area study and increased in equal areas with less than 10 Mg/ha. Thus, biomass growth (0–30 Mg/ha) is only recorded in limited small areas, barely exceeding 5% of the territory.



**Figure 8.** Change map of cork oak biomass (a) and carbon stock (b) between 1985 and 2020.

The spatialization of the carbon stock model is performed using Equation (20) (Table 3). Figure 9 shows the carbon stock distribution of cork oak in the study area in 2020 and 1985. The carbon stock distribution follows the same trend as the biomass (Figure 7). In 2020, very little carbon stock (less than 6 Mg/ha) covered most of the study area (about 80%), low carbon stock between 6 and 18 Mg/ha covered the rest, and in 1985, very little carbon stock covered a larger area, more than 90% of the study area. The changes in carbon stock in the study area between 1985 and 2020 are shown in Figure 8. This figure shows that the carbon stock decreased in some zones and increased slowly by less than 10 Mg/ha.

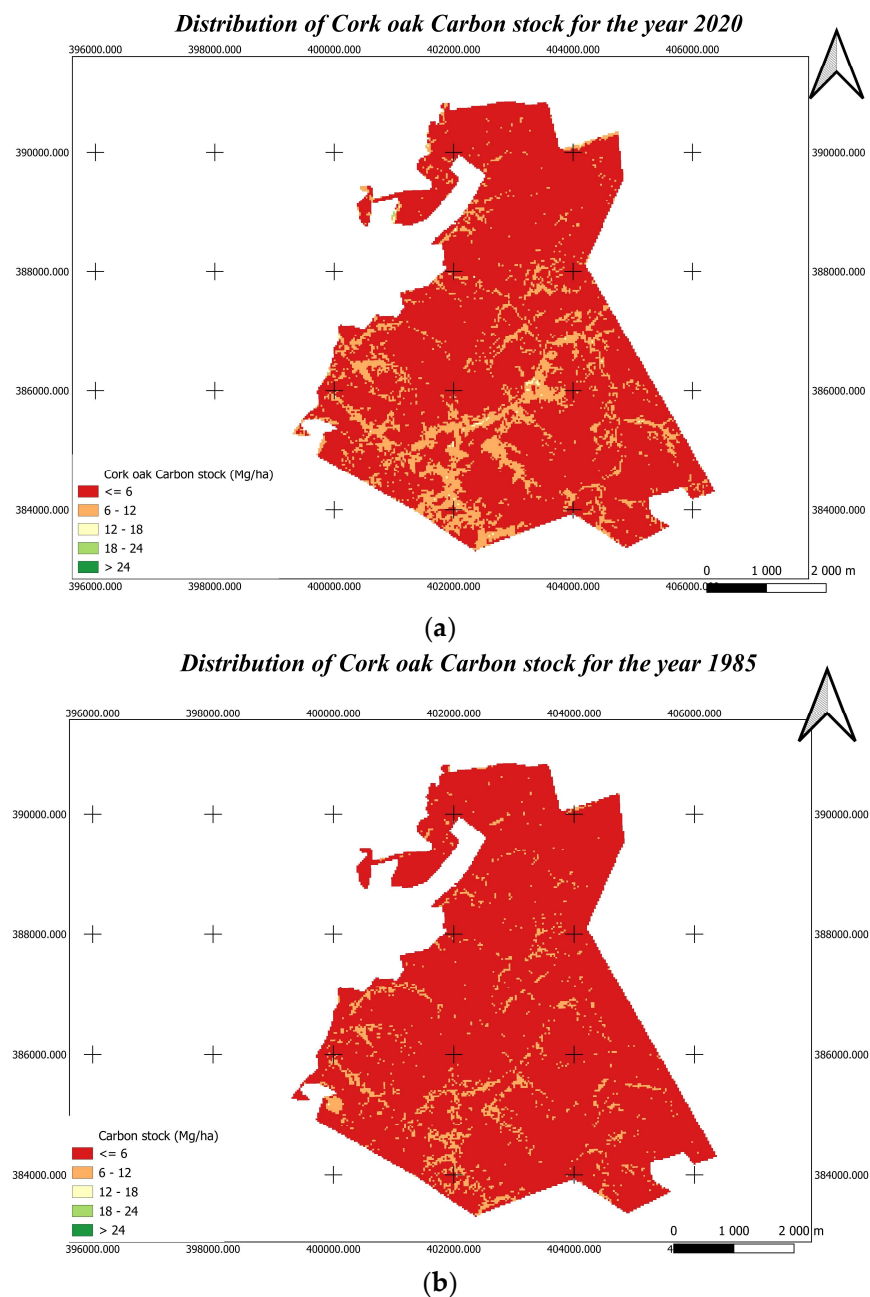


**Figure 9.** Distribution of cork oak carbon stock for 2020 (a) and 1985 (b).

#### 4. Discussion

Recent research has demonstrated the use of multisource data frameworks worldwide [18,62]. However, none of them has studied the cork oak species in the Mediterranean context or proposed a hierarchical three-phase methodology linked to three scales (plot, LiDAR UAV survey and landscape). In this sense, this study proposes a multidimensional framework, integrating field survey and new technologies such as UAV and LiDAR, and satellite imagery (Landsat images).

The Maamora forest was the largest cork oak forest in the world, covering more than 134,000 ha, including 60,000 ha of cork oak [49]. Unfortunately, this forest cover has shown decline in 1975, 1990, and 2022 [63]. Our results confirm the degraded condition of this forest. The main degradation factors are natural and anthropogenic. Indeed, the population of the Maamora forest is characterized by high human density, 50 inhabitants per km<sup>2</sup>, with a user population of 27,255 households spread over 15 rural communities [64]. The forest rangelands of this forest suffer from overexploitation with a demand of three to five

times that of forage potential and constitute an exclusive forage resource for extensive livestock, cattle, and sheep. The regional energy balance is largely dependent on wood energy from forests, which accounts for 67% of the wood energy consumed annually [64]. The strategic location of this forest has made it vulnerable to uncontrolled urbanization, particularly as a result of excessive use for recreational purposes and land clearing for major development projects such as motorways. Since the early 20th century (1918), the Maamora forest has been the subject of several forest management plans, which have recommended the introduction of exotic species, the involvement of the local population and the regeneration of cork oaks by seeding or planting, but the objective of conserving and perpetuating this forest has still not been achieved. Natural factors are also partly to blame, such as fires, insect pests, aging of the stands, and recurrent droughts [65], climate change, and decrease in stand tree density (<100 trees/ha) [48], etc. Thus, the combination of all these factors has led to the degradation of the Maamora forest, which is reflected in its range [66], biodiversity, stand structure, and tree density.

Few studies have dealt with the quantification of biomass and carbon stocks in the Maamora forest using traditional or new technology methods [7,48]. In this forest, the study of forest land use and land cover change between 1987 and 2020 showed that there was an increase in bare land, agricultural land, and built areas to the detriment of the forest area [67]. However, no study has investigated the likely changes in biomass and carbon stock, despite their importance in understanding the carbon sequestration process. Cork oak habitat distribution maps are related to current and future climate conditions in different scenarios [68]. In this context, the present research allows a spatialization of biomass and carbon stock, which is crucial for the identification of priority areas requiring intervention by local managers, and a better knowledge of biomass and carbon stock dynamics, thus informing us about past rate changes and allowing us to predict the rate of future changes.

The results of vegetation index comparison (ARVI, NDVI, and CIG) using simple and stepwise linear regression shows that the ARVI is the best, with a slight difference from NDVI and CIG. Indeed, the most common vegetation index used in canopy monitoring and biomass assessment is the NDVI [69]. However, because the NDVI is susceptible to various outside influences such as atmospheric disturbance, other vegetation indices were developed, in particular the ARVI, which is most useful in regions of high atmospheric aerosol content. It uses blue light reflectance measurements to correct for the atmospheric scattering effects that also influence the reflectance of red light [70]. The use of this vegetation index in biomass modeling in different landscapes and various forest stands is proven by other research [71–73].

## 5. Conclusions

In this study, the general objective was to spatialize biomass and carbon stocks on a large scale and to analyze their dynamics using an innovative methodological approach, and the specific objectives were (i) to explore the potential of vegetation indices from Landsat images in biomass and carbon stock modeling, (ii) to analyze and compare different regression types, including ML techniques (random forest regression), and (iii) to assess biomass and carbon stock changes in a Mediterranean cork oak forest stand. For this purpose, a new approach combining forest survey data, LiDAR UAV data and extracted Landsat 8 images vegetation indices (NDVI, ARVI, CIG, etc.) was used. Different regression types (univariate and multivariate) were used, such as multiple linear regression, stepwise linear regression, random forest regression, simple linear regression, logarithmic regression, and quadratic and cubic regression.

The results show that stepwise regression and random forest regression give good results, explaining a good part of the variation in biomass and carbon stock. Univariate regression using simple linear regression gives satisfactory results, close to those of quadratic and cubic regression, but with a simpler equation. The vegetation index chosen is the ARVI, which shows good performance indices, close to those of the NDVI and CIG. The

assessment of biomass and carbon stock changes in the study area over 35 years (1985–2020) showed a slight increase of less than 10 Mg/ha and a large decrease in biomass and carbon stock over a wide area.

**Author Contributions:** Conceptualization, S.F. and I.S.; methodology S.F. and I.S.; software, Y.Z., R.A., I.E.M., K.A.E.k. and M.J.; validation, I.S. and M.M.A.; formal analysis, S.F. and M.M.A.; investigation, S.F., I.S. and K.A.E.k.; resources, I.S. and K.A.E.k.; data curation, S.F.; writing—original draft preparation, S.F.; writing—review and editing, S.F. and I.S.; visualization, S.F.; supervision, I.S.; project administration, I.S. All authors have read and agreed to the published version of the manuscript.

**Funding:** This research received no external funding.

**Data Availability Statement:** Data are contained within the article.

**Acknowledgments:** The authors express their gratitude to El Ghoudani Driss for his valuable contribution in the field data acquisition.

**Conflicts of Interest:** The authors declare that they have no known competing financial interests or personal relationships that could have appeared to influence the work reported in this paper.

## References

1. FAO. *In Brief to The State of the World's Forests 2022*; FAO: Rome, Italy, 2022; Available online: <https://openknowledge.fao.org/handle/20.500.14283/cb9363en> (accessed on 24 April 2024).
2. Zhang, H.; Liu, S.; Yu, J.; Li, J.; Shangguan, Z.; Deng, L. Thinning increases forest ecosystem carbon stocks. *For. Ecol. Manag.* **2024**, *555*, 121702. [CrossRef]
3. Dixon, R.K.; Winjum, J.K.; Andrasko, K.J.; Lee, J.J.; Schroeder, P.E. Integrated land-use systems: Assessment of promising agroforest and alternative land-use practices to enhance carbon conservation and sequestration. *Clim. Change* **1994**, *27*, 71–92. [CrossRef]
4. Seidl, R.; Thom, D.; Kautz, M.; Martin-Benito, D.; Peltoniemi, M.; Vacchiano, G.; Wild, J.; Ascoli, D.; Petr, M.; Honkaniemi, J.; et al. Forest disturbances under climate change. *Nat. Clim. Change* **2017**, *7*, 395–402. [CrossRef] [PubMed]
5. IPCC. IPCC\_AR6\_WGII\_FinalDraft\_FullReport.pdf. Available online: [https://report.ipcc.ch/ar6wg2/pdf/IPCC\\_AR6\\_WGII\\_FinalDraft\\_FullReport.pdf](https://report.ipcc.ch/ar6wg2/pdf/IPCC_AR6_WGII_FinalDraft_FullReport.pdf) (accessed on 3 May 2022).
6. FORESTS—Climate Change, Biodiversity and Land Degradation. p. 12.
7. Sanaa, F.; Imane, S.; Mohamed, B.; El kadi Kenza, A.; Souhail, K.; Lfalah, H.; Khadija, M. Biomass and Carbon Stock Quantification in Cork Oak Forest of Maamora Using a New Approach Based on the Combination of Aerial Laser Scanning Carried by Unmanned Aerial Vehicle and Terrestrial Laser Scanning Data. *Forests* **2022**, *13*, 1211. [CrossRef]
8. Gesta, J.L.E.; Fernandez, J.M.; Lina, R.S.; Santillan, J.R. Aboveground biomass and carbon stock estimation of falcata through the synergistic use of sentinel-1 and sentinel-2 images. *Int. Arch. Photogramm. Remote Sens. Spat. Inf. Sci.* **2023**, *48*, 117–122. [CrossRef]
9. Brede, B.; Terry, L.; Barbier, N.; Bartholomeus, H.M.; Bartolo, R.; Calders, K.; Derroire, G.; Krishna Moorthy, S.M.; Lau, A.; Levick, S.R.; et al. Non-destructive estimation of individual tree biomass: Allometric models, terrestrial and UAV laser scanning. *Remote Sens. Environ.* **2022**, *280*, 113180. [CrossRef]
10. Loh, H.Y.; James, D.; Ioki, K.; Wong, W.V.C.; Tsuyuki, S.; Phua, M.-H. Estimating aboveground biomass changes in a human-modified tropical montane forest of Borneo using multi-temporal airborne LiDAR data. *Remote Sens. Appl. Soc. Environ.* **2022**, *28*, 100821. [CrossRef]
11. Hermans, K.; Jobbagy, E.; Kurz, W.; Li, D.; Sonwa, D.J.; Stringer, L.; Haughey, E.; Houghton, R.; Lee, W.-K.; Morton, J. Chapter 4: Land Degradation. In *Special Report: Special Report on Climate Change and Land*; IPCC: Geneva, Switzerland, 2019; p. 157.
12. Wang, Y.; Jia, X.; Chai, G.; Lei, L.; Zhang, X. Improved estimation of aboveground biomass of regional coniferous forests integrating UAV-LiDAR strip data, Sentinel-1 and Sentinel-2 imageries. *Plant Methods* **2023**, *19*, 65. [CrossRef]
13. Ningthoujam, R.K.; Joshi, P.K.; Roy, P.S. Retrieval of forest biomass for tropical deciduous mixed forest using ALOS PALSAR mosaic imagery and field plot data. *Int. J. Appl. Earth Obs. Geoinformation* **2018**, *69*, 206–216. [CrossRef]
14. Ali Hussin, Y. Assessment and Modelling of Forest Biomass and Carbon Stock and Sequestration Using Various Remote Sensing Sensor Systems. In *Concepts and Applications of Remote Sensing in Forestry*; Suratman, M.N., Ed.; Springer Nature: Singapore, 2022; pp. 75–95. [CrossRef]
15. Herold, M.; Johns, T. Linking requirements with capabilities for deforestation monitoring in the context of the UNFCCC-REDD process. *Environ. Res. Lett.* **2007**, *2*, 045025. [CrossRef]
16. Goetz, S.; Dubayah, R. Advances in remote sensing technology and implications for measuring and monitoring forest carbon stocks and change. *Carbon Manag.* **2011**, *2*, 231–244. [CrossRef]
17. Drake, J.B.; Knox, R.G.; Dubayah, R.O.; Clark, D.B.; Condit, R.; Blair, J.B.; Hofton, M. Above-ground biomass estimation in closed canopy Neotropical forests using lidar remote sensing: Factors affecting the generality of relationships. *Glob. Ecol. Biogeogr.* **2003**, *12*, 147–159. [CrossRef]

18. Wang, D.; Wan, B.; Liu, J.; Su, Y.; Guo, Q.; Qiu, P.; Wu, X. Estimating aboveground biomass of the mangrove forests on northeast Hainan Island in China using an upscaling method from field plots, UAV-LiDAR data and Sentinel-2 imagery. *Int. J. Appl. Earth Obs. Geoinformation* **2020**, *85*, 101986. [CrossRef]
19. Fadil, S.; Sebari, I.; Bouhaloua, M.; Kadi, K.A.E. Opportunités d'utilisation de la technologie drone au niveau des écosystèmes forestiers. *Rev. Marocaine Sci. Agron. Vét.* **2020**, *8*. Available online: [https://www.agrimaroc.org/index.php/Actes\\_IJVH2/article/view/888](https://www.agrimaroc.org/index.php/Actes_IJVH2/article/view/888) (accessed on 12 October 2023).
20. Alvarez-Vanhard, E.; Corpetti, T.; Houet, T. UAV & satellite synergies for optical remote sensing applications: A literature review. *Sci. Remote Sens.* **2021**, *3*, 100019. [CrossRef]
21. Dalla Corte, A.P.; Rex, F.E.; de Almeida, D.R.A.; Sanquetta, C.R.; Silva, C.A.; Moura, M.M.; Wilkinson, B.; Zambrano, A.M.A.; da Cunha Neto, E.M.; Veras, H.F.P.; et al. Measuring Individual Tree Diameter and Height Using GatorEye High-Density UAV-Lidar in an Integrated Crop-Livestock-Forest System. *Remote Sens.* **2020**, *12*, 863. [CrossRef]
22. Qin, S.; Wang, H.; Li, X.; Gao, J.; Jin, J.; Li, Y.; Lu, J.; Meng, P.; Sun, J.; Song, Z.; et al. Enhancing Landsat image based aboveground biomass estimation of black locust with scale bias-corrected LiDAR AGB map and stratified sampling. *Geo-Spat. Inf. Sci.* **2023**, *1–14*. [CrossRef]
23. Simula, M. Towards defining forest degradation: Comparative analysis of existing definitions. *For. Resour. Assess. Work. Pap.* **2009**, *154*, 59.
24. Berninger, A.; Lohberger, S.; Stängel, M.; Siegert, F. SAR-Based Estimation of Above-Ground Biomass and Its Changes in Tropical Forests of Kalimantan Using L- and C-Band. *Remote Sens.* **2018**, *10*, 831. [CrossRef]
25. Johnson, L.K.; Mahoney, M.J.; Desrochers, M.L.; Beier, C.M. Mapping historical forest biomass for stock-change assessments at parcel to landscape scales. *For. Ecol. Manag.* **2023**, *546*, 121348. [CrossRef]
26. Houghton, J. *Global Warming: The Complete Briefing*; Cambridge University Press: Cambridge, UK, 2009.
27. Lee, J.-H.; Im, J.-H.; Kim, K.-M.; Heo, J. Change Analysis of Aboveground Forest Carbon Stocks According to the Land Cover Change Using Multi-Temporal Landsat TM Images and Machine Learning Algorithms. *J. Korean Assoc. Geogr. Inf. Stud.* **2015**, *18*, 81–99. [CrossRef]
28. Nguyen, L.D.; Nguyen, C.T.; Le, H.S.; Tran, B.Q. Mangrove Mapping and Above-Ground Biomass Change Detection using Satellite Images in Coastal Areas of Thai Binh Province, Vietnam. *For. Soc.* **2019**, *3*, 248. [CrossRef]
29. Bera, B.; Bhattacharjee, S.; Sengupta, N.; Shit, P.K.; Adhikary, P.P.; Sengupta, D.; Saha, S. Significant reduction of carbon stocks and changes of ecosystem service valuation of Indian Sundarban. *Sci. Rep.* **2022**, *12*, 7809. [CrossRef] [PubMed]
30. Qu, R.; He, L.; He, Z.; Wang, B.; Lyu, P.; Wang, J.; Kang, G.; Bai, W. A Study of Carbon Stock Changes in the Alpine Grassland Ecosystem of Zoigê, China, 2000–2020. *Land* **2022**, *11*, 1232. [CrossRef]
31. Massada, A.B.; Carmel, Y.; Tzur, G.E.; Grünzweig, J.M.; Yakir, D. Assessment of temporal changes in aboveground forest tree biomass using aerial photographs and allometric equations. *Can. J. For. Res.* **2006**, *36*, 2585–2594. [CrossRef]
32. Ota, T.; Ogawa, M.; Shimizu, K.; Kajisa, T.; Mizoue, N.; Yoshida, S.; Takao, G.; Hirata, Y.; Furuya, N.; Sano, T.; et al. Aboveground Biomass Estimation Using Structure from Motion Approach with Aerial Photographs in a Seasonal Tropical Forest. *Forests* **2015**, *6*, 3882–3898. [CrossRef]
33. Chen, W.; Zheng, Q.; Xiang, H.; Chen, X.; Sakai, T. Forest Canopy Height Estimation Using Polarimetric Interferometric Synthetic Aperture Radar (PolInSAR) Technology Based on Full-Polarized ALOS/PALSAR Data. *Remote Sens.* **2021**, *13*, 174. [CrossRef]
34. Solberg, S.; Næsset, E.; Gobakken, T.; Bollandsås, O.-M. Forest biomass change estimated from height change in interferometric SAR height models. *Carbon Balance Manag.* **2014**, *9*, 5. [CrossRef] [PubMed]
35. Meyer, V.; Saatchi, S.S.; Chave, J.; Dalling, J.W.; Bohlman, S.; Fricker, G.A.; Robinson, C.; Neumann, M.; Hubbell, S. Detecting tropical forest biomass dynamics from repeated airborne lidar measurements. *Biogeosciences* **2013**, *10*, 5421–5438. [CrossRef]
36. Englhart, S.; Jubanski, J.; Siegert, F. Quantifying Dynamics in Tropical Peat Swamp Forest Biomass with Multi-Temporal LiDAR Datasets. *Remote Sens.* **2013**, *5*, 2368–2388. [CrossRef]
37. Zhao, K.; Suarez, J.C.; Garcia, M.; Hu, T.; Wang, C.; Londo, A. Utility of multitemporal lidar for forest and carbon monitoring: Tree growth, biomass dynamics, and carbon flux. *Remote Sens. Environ.* **2018**, *204*, 883–897. [CrossRef]
38. Wang, V.; Gao, J.; Schwendenmann, L. Assessing changes of urban vegetation cover and aboveground carbon stocks using LiDAR and Landsat imagery data in Auckland, New Zealand. *Int. J. Remote Sens.* **2020**, *41*, 2140–2158. [CrossRef]
39. Rappaport, D.I.; Morton, D.C.; Longo, M.; Keller, M.; Dubayah, R.; dos-Santos, M.N. Quantifying long-term changes in carbon stocks and forest structure from Amazon forest degradation. *Environ. Res. Lett.* **2018**, *13*, 065013. [CrossRef]
40. Maeda, Y.; Fukushima, A.; Imai, Y.; Tanahashi, Y.; Nakama, E.; Ohta, S.; Kawazoe, K.; Akune, N. Estimating carbon stock changes of mangrove forests using satellite imagery and airborne lidar data in the south sumatra state, indonesia. *Int. Arch. Photogramm. Remote Sens. Spat. Inf. Sci.* **2016**, *41*, 705–709. [CrossRef]
41. Ahmad, N.; Ullah, S.; Zhao, N.; Mumtaz, F.; Ali, A.; Ali, A.; Tariq, A.; Kareem, M.; Imran, A.B.; Khan, I.A.; et al. Comparative Analysis of Remote Sensing and Geo-Statistical Techniques to Quantify Forest Biomass. *Forests* **2023**, *14*, 379. [CrossRef]
42. Meliho, M.; Boulmane, M.; Khattabi, A.; Dansou, C.E.; Orlando, C.A.; Mhammdi, N.; Noumonvi, K.D. Spatial Prediction of Soil Organic Carbon Stock in the Moroccan High Atlas Using Machine Learning. *Remote Sens.* **2023**, *15*, 2494. [CrossRef]
43. Zhang, L.; Zhang, X.; Shao, Z.; Jiang, W.; Gao, H. Integrating Sentinel-1 and 2 with LiDAR data to estimate aboveground biomass of subtropical forests in northeast Guangdong, China. *Int. J. Digit. Earth* **2023**, *16*, 158–182. [CrossRef]

44. Lyu, X.; Li, X.; Gong, J.; Li, S.; Dou, H.; Dang, D.; Xuan, X.; Wang, H. Remote-sensing inversion method for aboveground biomass of typical steppe in Inner Mongolia, China. *Ecol. Indic.* **2021**, *120*, 106883. [[CrossRef](#)]
45. Jia, Z.; Zhang, Z.; Cheng, Y.; Buhebaoyin; Borjigin, S.; Quan, Z. Grassland biomass spatiotemporal patterns and response to climate change in eastern Inner Mongolia based on XGBoost model estimates. *Ecol. Indic.* **2024**, *158*, 111554. [[CrossRef](#)]
46. Velasco Pereira, E.A.; Varo Martínez, M.A.; Ruiz Gómez, F.J.; Navarro-Cerrillo, R.M. Temporal Changes in Mediterranean Pine Forest Biomass Using Synergy Models of ALOS PALSAR-Sentinel 1-Landsat 8 Sensors. *Remote Sens.* **2023**, *15*, 3430. [[CrossRef](#)]
47. Cao, Y.; Chen, Y. Biomass, Carbon and Nutrient Storage in a 30-Year-Old Chinese Cork Oak (*Quercus variabilis*) Forest on the South Slope of the Qinling Mountains, China. *Forests* **2015**, *6*, 1239–1255. [[CrossRef](#)]
48. Oubrahim, H.; Boulmane, M.; Bakker, M.R.; Augusto, L.; Halim, M. Carbon storage in degraded cork oak (*Quercus suber*) forests on flat lowlands in Morocco. *IForest—Biogeosci. For.* **2015**, *9*, 125–137. [[CrossRef](#)]
49. A Afi, A.; El Kadmiri, A.A.; Benabid, A.; Rochdi, M. Richesse et diversité floristique de la suberaie de la Mamora (Maroc). *Acta Bot. Malacit.* **2005**, *30*, 127–138. [[CrossRef](#)]
50. et Kaufman, Y.J.; Tanre, D. Atmospherically resistant vegetation index (ARVI) for EOS-MODIS. *IEEE Trans. Geosci. Remote Sens.* **1992**, *30*, 261–270. [[CrossRef](#)]
51. Dw, D. Measuring forage production of grazing units from Landsat MSS data. *Environ. Sci. Agric. Food Sci.* **1975**, 1169–1178.
52. Gitelson, A.A. Remote estimation of fraction of radiation absorbed by photosynthetically active vegetation: Generic algorithm for maize and soybean. *Remote. Sens. Lett.* **2018**, *10*, 283–291. [[CrossRef](#)]
53. Jordan, C.F. *Derivation of Leaf-Area Index from Quality of Light on the Forest Floor—Jordan—1969—Ecology*; Wiley Online Library: Hoboken, NJ, USA, 2024. Available online: <https://esajournals.onlinelibrary.wiley.com/doi/abs/10.2307/1936256> (accessed on 24 April 2024).
54. Huete, A.; Didan, K.; Miura, T.; Rodriguez, E.P.; Gao, X.; Ferreira, L.G. Overview of the radiometric and biophysical performance of the MODIS vegetation indices. *Remote Sens. Environ.* **2002**, *83*, 195–213. [[CrossRef](#)]
55. Rouse, J.W.; Haas, R.H.; Deering, D.W.; Schell, J.A.; Harlan, J.C. *Monitoring the Vernal Advancement and Retrogradation (Green Wave Effect) of Natural Vegetation*; NASA: Washington, DC, USA, 1974; E75-10354. Available online: <https://ntrs.nasa.gov/citations/19750020419> (accessed on 24 April 2024).
56. Gitelson, A.A.; Merzlyak, M.N. Signature Analysis of Leaf Reflectance Spectra: Algorithm Development for Remote Sensing of Chlorophyll. *J. Plant Physiol.* **1996**, *148*, 494–500. [[CrossRef](#)]
57. Rondeaux, G.; Steven, M.; Baret, F. Optimization of soil-adjusted vegetation indices. *Remote Sens. Environ.* **1996**, *55*, 95–107. [[CrossRef](#)]
58. Huete, A.R. A soil-adjusted vegetation index (SAVI). *Remote Sens. Environ.* **1988**, *25*, 295–309. [[CrossRef](#)]
59. Random Forest. Data Analytics Post. Available online: <https://dataanalyticspost.com/Lexique/random-forest/> (accessed on 19 May 2020).
60. University, G. Bagging and Random Forests 3. Available online: <https://dodona.be/en/activities/1878300012/> (accessed on 31 January 2024).
61. Poudel, A.; Shrestha, H.L.; Mahat, N.; Sharma, G.; Aryal, S.; Kalakheti, R.; Lamsal, B. Modeling and Mapping of Aboveground Biomass and Carbon Stock Using Sentinel-2 Imagery in Chure Region, Nepal. *Int. J. For. Res.* **2023**, *2023*, 5553957. [[CrossRef](#)]
62. Jiao, Y.; Wang, D.; Yao, X.; Wang, S.; Chi, T.; Meng, Y. Forest Emissions Reduction Assessment Using Optical Satellite Imagery and Space LiDAR Fusion for Carbon Stock Estimation. *Remote Sens.* **2023**, *15*, 1410. [[CrossRef](#)]
63. Zahra, L.; Thami, D. Impact of urban dynamics and climate change on forest areas the Maamora forest in the city of Kenitra, Morocco. *Multidiscip. Sci. J.* **2024**, *6*, 2024123. [[CrossRef](#)]
64. HCEFLCD. Etude Socio-Economique. Révision de l'étude d'aménagement de la forêt de Maamora, vol 4, 2014.
65. Laaribya, S. A review analysis of the degradation of cork oak forests in North Atlantic, Morocco. *J. Biometry Stud.* **2023**, *3*, 54–59. [[CrossRef](#)]
66. Laaribya, S.; Alaoui, A. Contribution à l'évaluation de la pression pastorale dans la forêt de la Maamora. Parcours forestiers et surpâturage. *Nat. Technol. J.* **2014**, *C*, 39–50.
67. Malki, F.; Karkouri, J.A.; Sabir, M.; El Mderssa, M.; Dallahi, Y. Contribution of geomatics tools to the study of the spatio-temporal evolution of forest stands of the Maamora forest in the face of global changes. *E3S Web Conf.* **2022**, *337*, 01001. [[CrossRef](#)]
68. Benabou, A.; Moukrim, S.; Lahssini, S.; Aboudi, A.E.; Menzou, K.; Elmalki, M.; Madihi, M.E.; Rhazi, L. Impact of climate change on potential distribution of *Quercus suber* in the conditions of North Africa. *Biosyst. Divers.* **2022**, *30*, 289–294. [[CrossRef](#)]
69. Comparison of the NDVI, ARVI and AFRI Vegetation Index, Along with Their Relations with the AOD Using SPOT 4 Vegetation Data | Request PDF. Available online: [https://www.researchgate.net/publication/291839625\\_Comparison\\_of\\_the\\_NDVI\\_ARVI\\_and\\_AFRI\\_vegetation\\_index\\_along\\_with\\_their\\_relations\\_with\\_the\\_AOD\\_using\\_SPOT\\_4\\_vegetation\\_data](https://www.researchgate.net/publication/291839625_Comparison_of_the_NDVI_ARVI_and_AFRI_vegetation_index_along_with_their_relations_with_the_AOD_using_SPOT_4_vegetation_data) (accessed on 8 February 2024).
70. Atmospherically Resistant Vegetation Index (ARVI) | Sentinel Hub Custom Scripts. Available online: <https://custom-scripts.sentinel-hub.com/custom-scripts/sentinel-2/arvi/> (accessed on 8 February 2024).
71. Bayaraa, B.; Hirano, A.; Purevtseren, M.; Vandansambuu, B.; Damdin, B.; Natsagdorj, E. Applicability of different vegetation indices for pasture biomass estimation in the north-central region of Mongolia. *Geocarto Int.* **2022**, *37*, 7415–7430. [[CrossRef](#)]

72. Verma, R.K.; Sharma, L.K.; Bhaveshkumar, K.I.; Rathore, M.K. Assessment of Aboveground Biomass in a Tropical Dry Deciduous Forest Using PRISMA Data. *J. Indian Soc. Remote Sens.* **2024**, 1–10. [[CrossRef](#)]
73. Forests | Free Full-Text | Estimation of Aboveground Biomass for Different Forest Types Using Data from Sentinel-1, Sentinel-2, ALOS PALSAR-2, and GEDI. Available online: <https://www.mdpi.com/1999-4907/15/1/215> (accessed on 8 February 2024).

**Disclaimer/Publisher’s Note:** The statements, opinions and data contained in all publications are solely those of the individual author(s) and contributor(s) and not of MDPI and/or the editor(s). MDPI and/or the editor(s) disclaim responsibility for any injury to people or property resulting from any ideas, methods, instructions or products referred to in the content.